Neural Comput & Applic (2017) 28:375–390
DOI 10.1007/s00521-015-2071-0

ORIGINAL ARTICLE

A multiplier-less digital design of a bio-inspired stimulator to suppress synchronized regime in a large-scale, sparsely connected neural network

Soheila Nazari[1,2] · Karim Faez[1] · Mahmood Amiri[3]

Received: 3 April 2015 / Accepted: 5 October 2015 / Published online: 28 October 2015

Abstract Excessive synchronous firing of neurons is the sign of several neurological disorders such as Parkinson and epilepsy. In addition, growing evidence suggests that astrocytes have significant roles in neural synchronization. Drawing on these concepts and based on the latest studies, a bio-inspired stimulator which essentially is a dynamical model of the astrocyte biophysical model is proposed. The performance of the proposed bio-inspired stimulator is investigated on a large-scale, sparsely connected neural network which models a local cortical population. Next, a multiplier-less digital circuit for the bio-inspired stimulator is designed, and finally, the complete digital circuit of the closed-loop system is implemented in hardware on the ZedBoard development kit. Considering software simulations and hardware FPGA implementation, the proposed bio-inspired stimulator is able to prevent the hyper-synchronous neural firing in a network of excitatory and inhibitory neurons. Based on the obtained results, it is demonstrated that the proposed stimulator has a demand-controlled characteristic and can be a good candidate as a new deep brain stimulation (DBS) technique to effectively suppress the hyper-synchronous neural oscillations.

Keywords DBS · Synchronization · Digital implementation · Bio-inspired Stimulator

✉ Mahmood Amiri
ma.amiri@ece.ut.ac.ir

[1] Department of Electrical Engineering, Amirkabir University of Technology, Tehran, Iran

[2] Students Research Committee, Kermanshah University of Medical Sciences, Kermanshah, Iran

[3] Medical Biology Research Center, Kermanshah University of Medical Sciences, Parastar Ave., Kermanshah, Iran

1 Introduction

Synchronization processes with a precision in the millisecond have an important mechanism for neuronal signaling and information processing [1]. On the other hand, *epilepsy*, *Parkinson* and *schizophrenia* have been historically seen as the functional brain disorders associated with excessive synchronization of neuronal cortical populations leading to a hyper-synchronous state [2, 3]. Hyper-synchrony has been traditionally associated with epilepsy, and it is interpreted as an epileptic activity, so that the most typical feature of epilepsy is hyper-synchronous activity of the neurons [4]. Epilepsy suffers 1 % of the world's population and is medically resisting in 30–40 % of cases [5]. A significant part (10–50 %) of medically refractory patients is candidates for respective surgery that postoperative improvement depending on the patient's condition is 40–90 %. [6]. Nevertheless, there are many patients who either cannot undergo respective surgery or, despite surgery, they have recurrent seizures [7]. A few number of them will respond to additional medication trials [8], and $<$10 % will achieve seizure freedom with vagus nerve stimulation after failed resection [9]. Thus, there is a real need for alternative therapies in medically refractory epilepsy. Deep brain stimulation (DBS) has proven remarkably effective, safe and practical in the treatment of patients with medically intractable neurological diseases [10].

Tukhlina and Rosenblum [11] proposed a linear feedback loop with a second-order filter that can provide an efficient suppression in the two interacting oscillatory networks. Simultaneously, the potential of delayed feedback stimulation as a novel method for the effective DBS via multiple sites to control the synchronization with demand-controlled de-synchronization technique is studied

in [12]. Recently, a feedback-based DBS has been tested in the model of Parkinson disease to show significantly greater effect of closed-loop DBS than standard open-loop DBS and matched control stimulation paradigms [13]. Despite recent proven efficacy in treating neurological disorders, such as Parkinson and epilepsy, DBS systems could be further optimized to maximize treatment benefits. Although current open-loop DBS strategies based on the fixed stimulation settings remove the rapid symptom variations partly uncontrolled, recent studies have focused on developing novel "closed-loop" DBS systems. Closed-loop DBS has been designed to measure and analyze a control variable which reflects the patient's clinical conditions to produce appropriate stimulation signal and then apply it to an implanted electrode. Choosing the ideal control variable for feedback in developing a closed-loop DBS system is the major problem. In accordance with [14], several practical and theoretical reasons confirm that local field potentials (LFP) correlate with the patient's clinical situation; therefore, here, we use this parameter as an input signal to the proposed stimulator. On the other hand, several findings support fundamental roles of astrocytes in stabilizing neural activities [15], and hence, the proposed stimulator as a new DBS technique is adapted from biophysical model of astrocyte.

Given that analog circuits are sensitive to fabrication process variations and very large-scale integrated (VLSI) implementation cannot be reconfigured easily [16, 17], it is necessary to have a rapid prototyping platform. Field-programmable gate arrays (FPGA) hardware is an ideal technology to achieve these requirements [18–22]. Here, first we use the astrocyte biophysical model as a stimulator. Next, in order to simplify the dynamic of the stimulator, we use a new astrocyte mathematical model as the stimulator. Finally, to achieve a simple and effective stimulator, we approximate astrocyte mathematical model and propose a new linear bio-inspired stimulator to be operated in a closed-loop DBS system. The digital design requirements of the three proposed stimulators are also compared and investigated. Moreover, a multiplier-less digital circuit of the proposed linear bio-stimulator is also implemented in hardware using ZedBoard development kit.

In order to evaluate the performance of the proposed stimulators, we designed a large-scale, sparsely connected cortical population model which has been adapted from the model introduced by [23]. It should be mentioned there are several experimental evidence which supports that the cortex has a primary role in seizure generation [24]. The cortical population model consisted of 8000 excitatory pyramidal neurons (PY) and 2000 inhibitory interneurons (IN) with 10 million excitatory and inhibitory synapses, so that this model is a suitable platform to evaluate the performance of the proposed bio-inspired stimulators.

The rest of this paper is organized as follows: The cortical population model and the bio-inspired stimulators are explained in Sects. 2 and 3, respectively. Digital designs of the bio-inspired stimulators are described in Sect. 4. Simulation results of the open-loop and closed-loop systems and hardware FPGA implementation are presented in Sect. 5. Finally, Sect. 6 concludes the paper.

2 Cortical population model

Developing computational model of cortical which is closely related to experimental data for studying epilepsy can markedly advance our understanding of essential issues in epilepsy [25, 26]. A method for studying epileptic brain is that we develop computational model considering the biological plausibility. Experimental studies confirmed that cortical networks support the emergence of epileptic activity remarkably. However, cortex and thalamus are responsible for generating the patterns of generalized seizures [27]. In this study, we consider cortical neural population model proposed by [23].

Model of cortical network consists of leaky integrate-and-fire neurons [23]. The network model has composed of two neuronal populations: 2000 inhibitory interneurons and 8000 pyramidal neurons. The network connectivity is random with 0.1 probability of directed connection between any pair of neurons, so that over 10 million excitatory and inhibitory synapses have considered in the network. All neurons are arranged in the form of a rectangular matrix with 100*100 arrays, and number of connections for individual neuron is shown in Fig. 1.

The simulated cortical network is composed of $N = 10{,}000$ neurons. Eighty percentage of the neurons are taken to be excitatory, and the remaining 20 % are inhibitory [23]. Both pyramidal neurons and interneurons are described by leaky integrate-and-fire (LIF) dynamics [28].

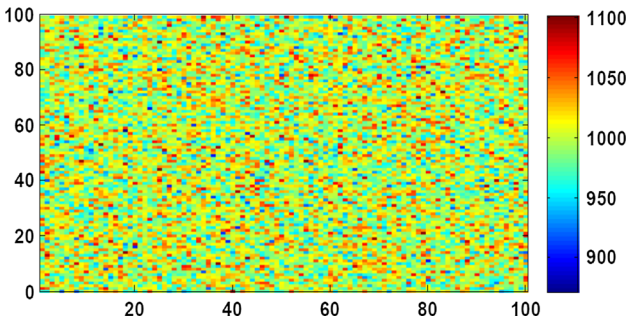

Fig. 1 The neuronal network is composed of two populations: interneurons and pyramidal neurons. There are 2000 interneurons and 8000 pyramidal neurons. The connectivity is random, and each point shows the number of connections for corresponding neuron

Each neuron k is described by its membrane potential $v_k(t)$ that describes as follows:

$$\tau_m \frac{dv_k}{dt} = -v_k(t) + I_{Ak}(t) - I_{Gk}(t) \quad (1)$$

where τ_m is the membrane time constant, I_{Ak} is the (AMPA-type) excitatory synaptic currents received by neuron k, I_{Gk} is the (GABA-type) inhibitory currents received by neuron k. When the membrane potential crosses the threshold, neuron cannot fire again for a refractory time.

We use LIF neuron model and consider more than 10 million excitatory and inhibitory synapses to create a complex connectivity structure for studying the effect of bio-inspired stimulator to control the hyper-synchronized neuronal activities. Thus, the complexity of the network is not limited to the large network of the LIF neurons, but also the main complexity of the designed network is considered in the synaptic connections. Synaptic currents can be obtained using auxiliary variables x_{Ak} and x_{Gk}. AMPA and GABA-type currents of neuron k are described as follows:

$$\tau_{dA} \frac{dI_{Ak}}{dt} = -I_{Ak} + x_{Ak} \quad (2)$$

$$\tau_{rA} \frac{dx_{Ak}}{dt} = -x_{Ak} + \tau_m \left(J_{k-Pyr} \sum_{Pyr} \delta(t - t_{k-pyr} - \tau_L) + J_{k-ext} \sum_{ext} \delta(t - t_{k-ext} - \tau_L) \right) \quad (3)$$

$$\tau_{dG} \frac{dI_{Gk}}{dt} = -I_{Gk} + x_s \quad (4)$$

$$\tau_{rG} \frac{dx_{AG}}{dt} = -x_{AG} + \tau_m \left(J_{k-int} \sum_{int} \delta(t - t_{k-int} - \tau_L) \right) \quad (5)$$

where $t_{k-pyr,int,ext}$ is the time of the spikes received from pyramidal neurons/interneurons connected to neuron k or from external inputs. $\tau_{dA}(\tau_{dG})$ and $\tau_{rA}(\tau_{rG})$ are, respectively, the decay and rise time of the AMPA-type (GABA-type) synaptic current. τ_L is the latency of post-synaptic currents. $J_{k-pyr,int,ext}$ is the efficacy of the connections from pyramidal neurons/interneurons/external inputs on neuron k. In order to consider the noise that is derived from the thalamus, we modeled noise component according to an Ornstein–Uhlenbeck process as follows:

$$\tau_n \frac{dn(t)}{dt} = -n(t) + \sigma_n \left(\sqrt{\frac{2}{\tau_n}} \right) \eta(t) \quad (6)$$

Here σ_n is the standard deviation of the noise, and $\eta(t)$ is a Gaussian white noise. Each neuron receives an external excitatory synaptic input that is considered with the random Poisson spike trains. Rate of excitatory input signal for each neuron is as follows:

$$v_{ext}(t) = \left[v_{signal}(t) + n(t) \right]_+ \quad (7)$$

In Eq. (7), $v_{signal}(t)$ represents the signal, and $n(t)$ is the noise. $[\ldots]$ is a threshold-linear function which defines by:

$$[x] = \begin{cases} x & \text{if } x < 0 \\ 0 & \text{if } x \leq 0 \end{cases} \quad (8)$$

Values of all parameters are taken from [23]. One of the interesting features of this oscillatory regime is that it strongly depends on external inputs. For weak external inputs, the network is typically in an asynchronous state. As the input increases, the network becomes more synchronized, and the amplitude of the oscillation increases [28]. We create abnormal synchronization in the cortical neuronal population with increase in the input.

Closed-loop DBS based on neuronal discharge patterns has better performance than standard open-loop DBS in improving patients with medically intractable neurological diseases such as Parkinson or epilepsy [14]. Research conducted over the past 10 years suggests that neuronal oscillations can also be reflected through recorded LFP [29]. LFPs can be recorded through the macro-electrodes implanted for DBS, reflect synchronous presynaptic and postsynaptic activity from local neuronal populations and oscillate in response to the patient's clinical state [30]. We computed the LFP as the sum of the absolute values of AMPA and GABA currents from synapses of the pyramidal neurons population [23, 31–33].

3 Bio-inspired stimulators

Astrocytes are the most abundant type of glial cells. They contain a plethora of ion channels, neurotransmitter receptors and transporters [34], and hence, they can listen and talk to synaptic activities by exerting both excitatory and inhibitory actions [35]. Astrocytes have now been recognized as active partners in neural information processing [36]. Later studies using more complete preparations confirmed the view that astrocytes are direct communication partners of neurons [37]. Astrocytes seem to be key players in fundamental brain functions, e.g., in learning and memory [38], control of sleep [39] and neuronal synchronization [40, 41]. Motivated by this finding, the dynamical model of astrocyte can be a good candidate as a stimulator to desynchronize hyper-synchronous firing of neurons [42]. In the rest of this section, we discuss on the astrocyte biophysical model, astrocyte mathematical model and a proposed simple model as a bio-inspired stimulator to be recruited in DBS.

3.1 First stimulator model: astrocyte biophysical model

To model the dynamics of the biophysical astrocyte model, we use the following set of equations to explain the intracellular calcium waves that are produced by astrocytes [43].

$$\tau_c \frac{dc}{dt} = -c - c_4 f(c, c_e) + (r + \beta S_m) \tag{9}$$

$$\varepsilon_c \tau_c \frac{dc_e}{dt} = f(c, c_e) \tag{10}$$

$$f(c, c_e) = c_1 \frac{c^2}{1 + c^2} - \left(\frac{c_e^2}{1 + c_e^2}\right)\left(\frac{c^4}{c_2^4 + c^4}\right) - c_3 c_e \tag{11}$$

$$\tau_{Sm} \frac{dS_m}{dt} = (1 + \tanh[S_{Sm}(z - h_{Sm})]) \times (1 - S_m) - \frac{S_m}{d_{Sm}} \tag{12}$$

$$\tau_{G_m} \frac{dG_m}{dt} = (1 + \tanh[S_{G_m}(c - h_{G_m})]) \times (1 - G_m) - \frac{G_m}{d_{G_m}} \tag{13}$$

where c and c_e define the calcium concentration within the astrocyte and internal store (ER), respectively. The calcium influx from the extracellular space into the cytoplasm is denoted by $r + \beta_{Sm}$ where β controls production of secondary messenger, and the reaction of astrocyte against firing of neuron is dependent on this parameter, so that with increase or decrease in β we can see the different speeds in astrocyte response. Two-variable function $f(c, c_e)$ has been defined to describe the calcium exchange between the cytoplasm and the endoplasmic reticulum. Here the S_m variable has been considered to define the changing concentration of IP_3 and the production of glial glutamate is denoted by G_m variable. The values of parameters have been listed in Table 1 [19, 43]. The interaction between astrocyte and neuronal populations is denoted by the parameter Z (bio-inspired stimulator input) that shows the synaptic activity of the cortical population. According to [23, 31–33], we computed the LFP as the sum of the absolute values of AMPA currents and GABA currents from synapses of the pyramidal neurons population. Scientific research provides robust evidence about correlation between LFP oscillations and the patient's clinical state [14], so here we considered scaled version of the LFP as an input control variable (Z) to the stimulator:

$$Z = a \times \text{LFP} \times \exp(-kR_1) \tag{14}$$

where R_1 is the Euclidean distance between the recording electrode and the other neurons, a is a constant parameter and equal to 0.0000002. Scaled version of the stimulator output is a feedback to the cortical population model as follows:

$$i^{\text{stim}} = \lambda_1 \times G_m \times \exp(-kR_2) \tag{15}$$

where R_2 is the Euclidean distance between the stimulating electrode and the other neurons of the network and λ_1 is a constant parameter.

According to Fig. 2, all neurons are arranged in the form of rectangular matrix 100*100, in which the location of the recording and stimulating electrodes is (50, 60) and (50, 40), respectively. Each neuron in this figure is shown by red ellipse.

The general scheme of the closed-loop DBS system is shown in Fig. 3. As is evident from this figure, recorded LFP from neuronal population is the input (Z) of the bio-inspired stimulator and its output is applied to the cortical population.

Table 1 Parameter values of the astrocyte biophysical model used in the simulations

Astrocyte parameters			
T_c	2	T_{sm}	10
c_1	0.13	d_{sm}	0.071
c_2	0.9	S_{sm}	100
c_3	0.004	h_{sm}	0.015
c_4	100	T_{Gm}	1.5
ε_c	0.01	d_{Gm}	2.5
r	0.02	S_{Gm}	100
β	1	h_{Gm}	0.025

3.2 Second stimulator model: astrocyte mathematical model

Montaseri and Yazdanpanah in [44] proposed a mathematical model based on the biophysical model of the astrocyte dynamics. Despite some simplifications, the main and essential properties of the biophysical astrocyte model are preserved in the structure of the simplified mathematical model. In this paper, the dynamics of the stimulator which has been inspired from the astrocyte mathematical model is defined with the following set of differential equations:

$$\dot{x} = -x + 0.05 + 1.5y \tag{16}$$

$$\dot{y} = [1 + \tanh(z - 2)](1 - y) - 2y \tag{17}$$

where y is the stimulator internal state and represents the production of secondary messenger within the astrocyte, x is the stimulator output which denotes calcium concentration within the astrocyte. The interaction between stimulator and neuronal population is denoted by the parameters Z (stimulator input) and i^{stim} (stimulator output

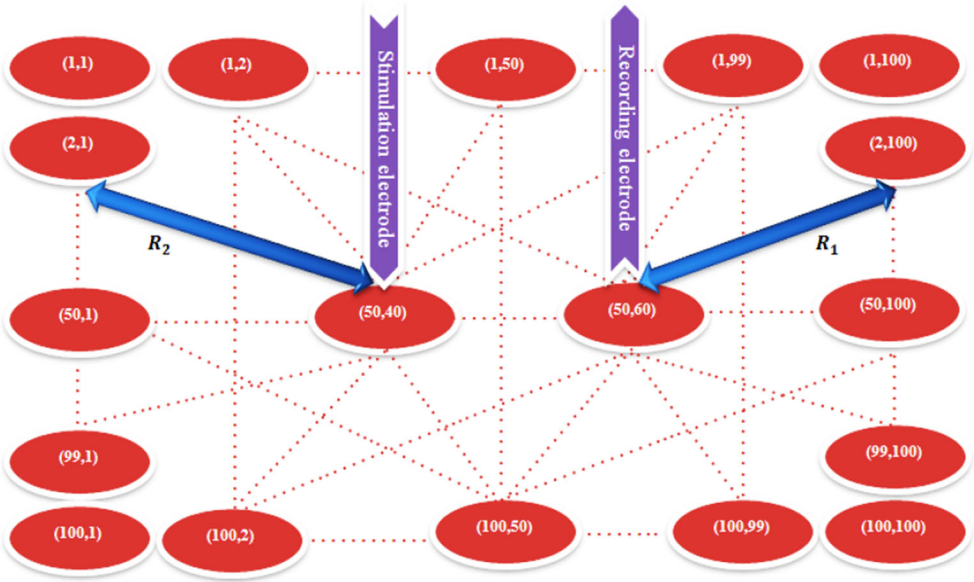

Fig. 2 Stimulation electrode is located in (50, 40), and recording electrode is placed at (50, 60) in the neural network. R_1 is the Euclidean distance between individual neurons and the recording electrode, and R_2 is the Euclidean distance between individual neurons and the stimulating electrode

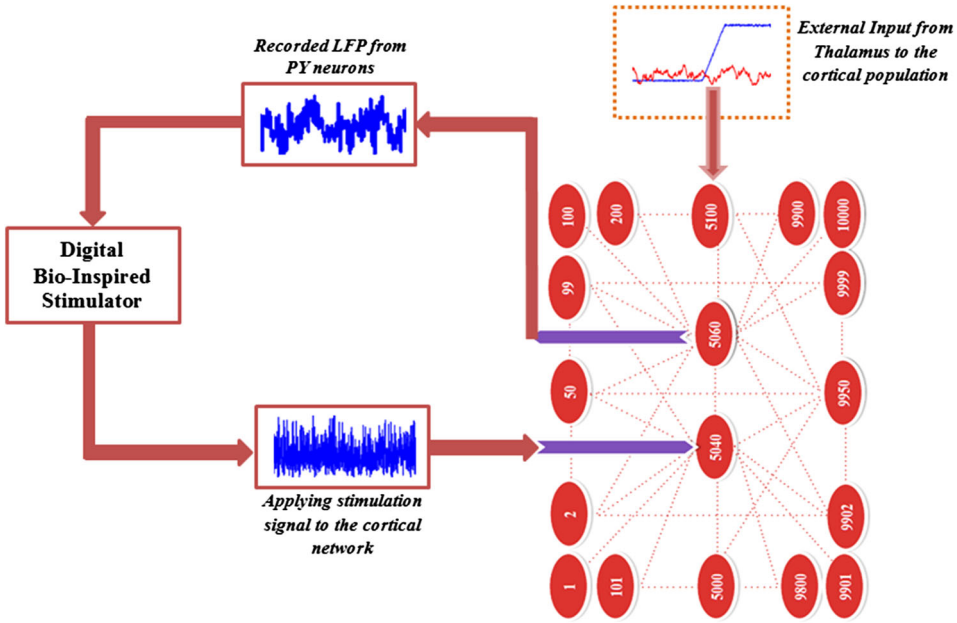

Fig. 3 The scheme of the closed-loop DBS system. It is composed of the cortical population model and a bio-inspired stimulator. LFP is the input control variable to the stimulator, and the stimulator output is a feedback to the cortical population model

signal) that Z has been defined in Eq. (14) and i^{stim} is defined as follows:

$$i^{\text{stim}} = \lambda_2 \times x \times \exp(-kR_2) \tag{18}$$

where R_2 is the Euclidean distance between the stimulating electrode and individual neurons and λ_2 is a constant parameter.

3.3 Third stimulator model: the proposed bio-stimulator

Designing a new stimulator by considering the feasibility of its implementation in the form of digital or analog circuits is the point that should be considered for real application of the deep brain stimulators. Whenever stimulator's equations become more simple, fabrication and implementation of these equations on the digital or analog platforms will become more possible [16–22]. Here, we propose a linear model for astrocyte mathematical model. In spite of linearization of the stimulator's equations, the stability analysis, which will be discussed in the following, shows that the main properties of the astrocyte mathematical model are preserved in the structure of the proposed stimulator.

In the proposed model, we replace nonlinear equation (Eq. 17) with linear equation. In order to achieve this goal,

we choose 30,000 random points ($m_i i = 1{:}30{,}000$) on the nonlinear surface (Eq. 17) and utilize surface-fitting method with least square error to reach the linear equation as follows:

$$y^{\cdot} = a_1 y + a_2 z + a_3 \tag{19}$$

In the process of approximation, we change the random points to obtain the linear equation that the equilibrium points of the approximated linear equation are equal to equilibrium points of the original nonlinear equation. So, we focus on the dynamic behavior of the system in the phase portrait.

In order to obtain the coefficients a_1, a_2, a_3, we must solve the following set of equations:

$$\begin{bmatrix} \sum_{i=1}^{30000} y_i^2 & \sum_{i=1}^{30000} y_i z_i & \sum_{i=1}^{30000} y_i \\ \sum_{i=1}^{30000} y_i z_i & \sum_{i=1}^{30000} z_i^2 & \sum_{i=1}^{30000} z_i \\ \sum_{i=1}^{30000} y_i & \sum_{i=1}^{30000} z_i & 1 \end{bmatrix} \begin{bmatrix} a_1 \\ a_2 \\ a_3 \end{bmatrix} = \begin{bmatrix} \sum_{i=1}^{30000} y_i m_i \\ \sum_{i=1}^{30000} z_i m_i \\ \sum_{i=1}^{30000} m_i \end{bmatrix} \tag{20}$$

So, the proposed linear model is as follows:

$$x^{\cdot} = -x + 0.05 + 1.5y \tag{21}$$

$$y^{\cdot} = 0.0937z - 2.035y + 0.03593 \tag{22}$$

The physiological meaning of the variable x, y in the proposed model is similar to the astrocyte mathematical model. Figure 4 shows the phase portrait of the astrocyte mathematical in (x–y) space (blue, dash) and the proposed model in (x–y) space (red, dash). It is clear that, in both systems, the phase portraits eventually converge to the same limit cycle. Therefore, it is expected that the proposed model has the similar dynamics to the astrocytes mathematical model [44].

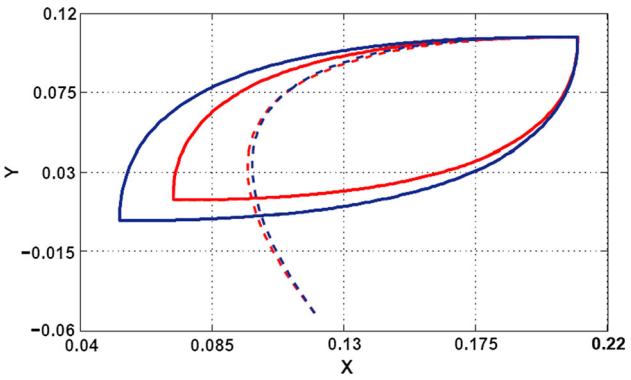

Fig. 4 Phase plane of the astrocyte mathematical model (*blue*, *dash*) and the proposed model (*red*, *dash*) in (x–y) space, when the input is set to square wave. The good similarity between the trajectories and limit cycles of both systems indicates the similar dynamics for both systems (color figure online)

To prove the accuracy of approximation in preserving the dynamic behavior of the system, we consider the important role of the two nullclines interactions [45]. The nullclines for two variables of the proposed stimulator are specified as follows:

$$x^{\cdot} = 0 \rightarrow -x + 0.05 + 1.5y = 0 \tag{23}$$

$$y^{\cdot} = 0 \rightarrow 0.0937z - 2.035y + 0.03593 = 0 \tag{24}$$

For obtaining the equilibrium point (the intersections of the x- and y-nullclines) of a dynamical system in the steady state, first we assume that the input (Z) is zero, so we have one fixed point with the coordinate $(x_{\text{eq}}, y_{\text{eq}}) = (0.07648,\ 0.01765)$. By computing the Jacobian matrix at this equilibrium point, the eigenvalues can be obtained.

$$J(x,y) = \begin{bmatrix} -1-\lambda & 1.5 \\ 0 & -2.035-\lambda \end{bmatrix} \rightarrow P(\lambda) = \lambda^2 + 3.035\lambda + 2.035 \tag{25}$$

Thus, we have : $(\lambda_1, \lambda_2) = (-1, -2.035)$ which means the equilibrium point is a stable node and attracts trajectories in the phase portrait. Similarly, in the original model [Eqs. (16), (17)], we obtain $(x_{\text{eq}}, y_{\text{eq}}) = (0.0765,\ 0.01766)$ and $(\lambda_1, \lambda_2) = (-1, -2.035)$. To illustrate the similarity of the dynamic behavior of proposed system in comparison with the original system, we plot the phase plane of the two systems considering $Z = 0$ in Fig. 5. Based on these results and Fig. 5, the proposed model without input has very similar behavior compared to the original model.

If the input of the proposed stimulator (Z) is not equal to zero, the equilibrium point is

$$x_{\text{eq}} = 0.069z + 0.07647 \tag{26}$$

$$y_{\text{eq}} = 0.046z + 0.01765 \tag{27}$$

By the coordinate transformation $\tilde{x} = x - x_{\text{eq}}$ and $\tilde{y} = y - y_{\text{eq}}$, the equilibrium point is shifted to the origin. In the new coordinates, the proposed model is represented with the $\tilde{x}$ (driven subsystem) and $\tilde{y}$ (driving subsystem) as the cascade system with the following equations:

$$\tilde{x}^{\cdot} = -\tilde{x} + 1.5\tilde{y} = f_1(\tilde{x}, \tilde{y}) \quad \tilde{y}^{\cdot} = -2.035\tilde{y} = f_2(\tilde{y}). \tag{28}$$

By considering the Lyapunov function $v_1 = 0.5\tilde{y}^2$, we have

$$v_1^{\cdot} = -2.035\tilde{y}^2 < -2\tilde{y}^2 \tag{29}$$

Therefore, $\tilde{y}^{\cdot}$-subsystem is globally exponentially stable. Next, since the unforced term of $\tilde{x}^{\cdot}$-subsystem (i.e., $\tilde{x}^{\cdot} = -\tilde{x}$) is globally exponentially stable, it is input-to-state stable with $\tilde{y}$ as an output (Lemma 4.6 in [46]). Finally, using Lemma 4.7 in [46], it is concluded that (0,0) is a globally asymptotically equilibrium point of the total system in Eq. (27). Thus, the stimulator is globally

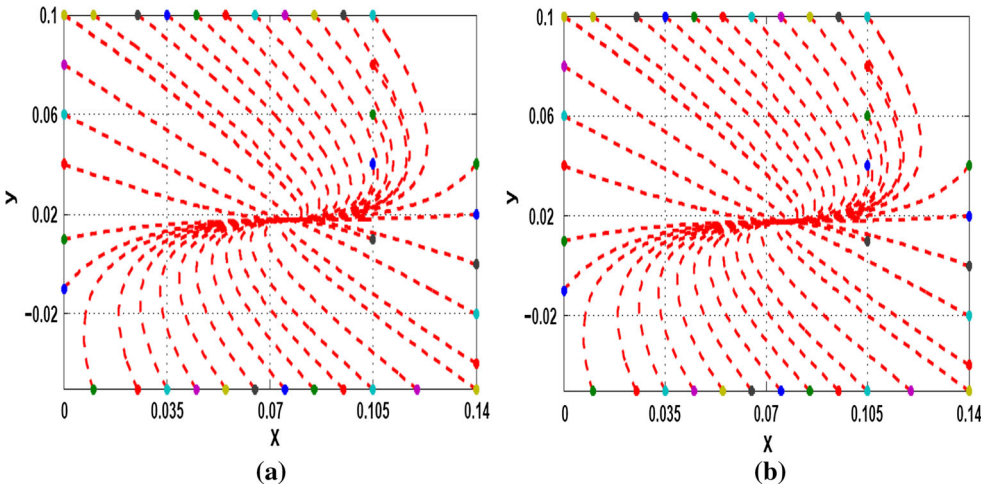

Fig. 5 The dynamic behavior of the original system and the proposed system in phase portrait considering zero as the input. **a** The phase plane of the original model when input is zero, and **b** the phase plane of the proposed model when input is zero. As can be seen in the original and proposed model, stable node attracts any points in the phase portrait

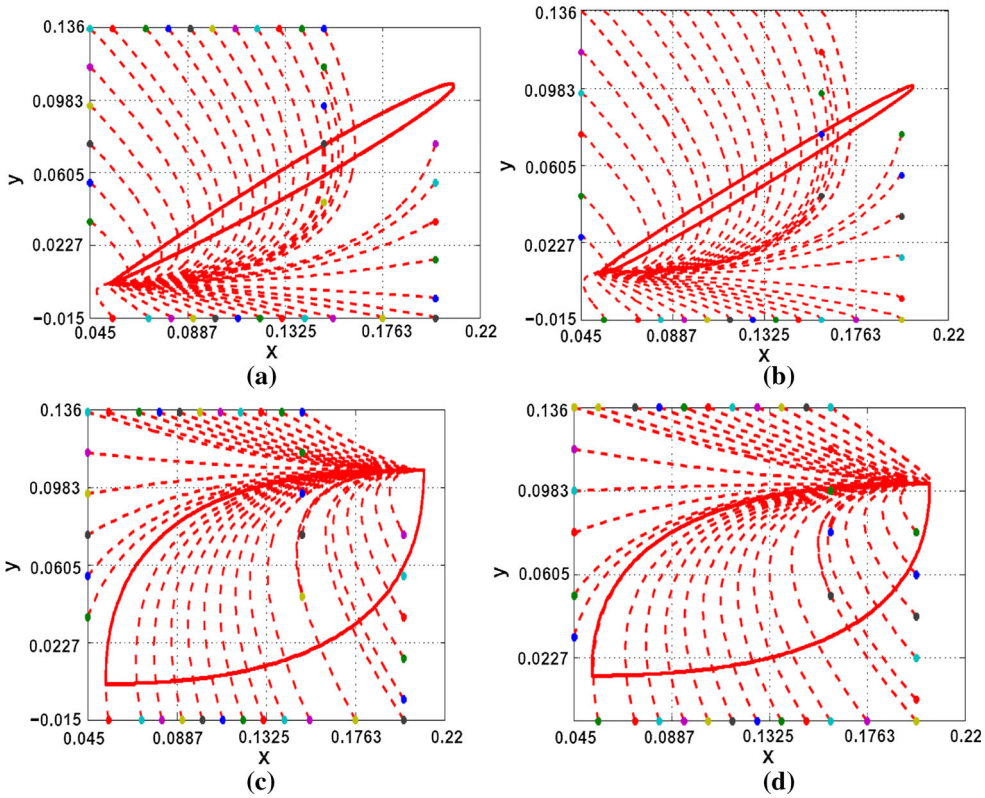

Fig. 6 The dynamic behavior of the original system and the proposed system in phase portrait considering the periodic signal as the input. **a**, **b** The phase plane of the original model and proposed model when input is $\sin(0.1t)$ and **c**, **d** the phase plane of the original model and proposed model when the input is $\text{square}(0.1t)$. As can be seen, the phase portrait of the original and proposed model is similar. Thus, the proposed model can follow the behavior of the original model

asymptotically stable. In order to clarify the above analysis, we express input-to-state stability concept, the Lyapunov-based theorem, Lemmas 4.6 and 4.7 from [46].

The dynamical behavior of the proposed model in comparison with the original model considering arbitrary inputs should be similar. Here we assume $z = \sin(0.1t)$ and $Z = \text{square}(0.1t)$, then plot trajectories for original and proposed model in Fig. 6 respectively. Root-mean-square error (RMSE) between trajectories of the original and proposed model is denoted in Table 2.

The main characteristic of the proposed stimulator is that it generates the proper stimulation current (i^{stim} in Eq. 30) based on the observation Z (Eq. 14) of the pyramidal neuronal population (see Sect. 5).

$$i^{\text{stim}} = \lambda_3 \times x \times \exp(-kR_2) \tag{30}$$

where R_2 is the Euclidean distance between the stimulating electrode (bio-inspired stimulator) and individual neurons and λ_3 is a constant parameter.

Table 2 RMSE between path of trajectories for the original and proposed model

RMSE		
$Z = 0$	$z = \sin(0.1t)$	$Z = \text{square}(0.1t)$
0.000015491	0.0203	0.0245

4 Digital design of the stimulators

FPGA consists of thousands of reconfigurable logic elements. The wiring that connects logic elements is electrically reconfigurable. Therefore, components can be wired together to create one design. Then, it can be erased and wired together differently to create a new one. Analog circuits are sensitive to fabrication process, and VLSI implementation cannot be reconfigured easily. Since FPGA is a digital device that owns reprogrammable properties and robust flexibility, many researchers have made great efforts on designing neuromorphic systems using FPGA technique [18–21, 47, 48]. Since a multiplier is an expensive block in terms of area and power consumption, in this research, we try to utilize simple blocks such as shifters and adders [20, 21]. This approach can help to reimburse the limited number of available fast multipliers on the chip. Single constant multiply (SCM) technique is used for efficient low-cost hardware implementation on digital platforms. In this way, we modify the coefficient constants so that they can be rewritten based on the power of 2. Indeed, it is possible to replace the multiplication with shift and add operations. On the other hand, fewer states are required to produce the output compared to the original model [21, 22]. The modified parameters using SCM technique are listed in Table 3 for astrocyte biophysical model. Here, we used linear approximation method and SCM technique to decrease the number of recruited multipliers and could design digital circuit for astrocyte biophysical and mathematical models using only one multiplier. In order to develop a low-cost and multiplierless digital circuit for the bio-inspired stimulator, we proposed a linear model for astrocyte mathematical model. According to Sect. 3.3 and simulation results which will be discussed in Sect. 5, it is evident that the proposed stimulator has the dynamic behavior similar to the astrocyte mathematical/biophysical model and it can prevent the pathological neuronal synchronization when the cortical input is high, and based on the synthesis results reported in Table 4, the new proposed stimulator required less resources in digital design which in turn reduces the digital implementation cost significantly.

Table 3 Modified parameter values of astrocyte dynamical model in the digital implementation

Astrocyte parameters			
T_c	2	T_{sm}	10
c_1	0.125	d_{sm}	0.071
c_2	1	S_{sm}	128
c_3	0.0039	h_{sm}	0.015
c_4	128	T_{Gm}	1.5
ε_c	0.0156	d_{Gm}	2.5
r	0.02	S_{Gm}	128
β	1	h_{Gm}	0.025

Table 4 High-level device utilization summary

Synthesis report	Astrocyte biophysical model	Astrocyte mathematical model	The proposed model
20*20-bit multipliers	1	1	0
20-bit adder/subtractor	6	2	2
Flip-flops	883	232	198
Comparators	12	5	0
Multiplexers	97	54	46
FSMs	1	1	1

The astrocyte biophysical and mathematical models and the new proposed model are discretized using Euler method with discretizing step (h) as 0.015625 (2^{-6}). The discrete equations of the astrocyte biophysical model are as follows [19]:

$$\begin{aligned} c[n+1] = (&-c[n] - c_4(c_1(A_2 * c[n] + B_2) \\ &-(A_2 * c_e[n] + B_2)(A_2 * c[n] * c[n] + B_2) \\ &-c_3 c_e[n]) + r + \beta s_m[n]) \times \frac{h}{\tau_c} + c[n] \end{aligned} \tag{31}$$

$$\begin{aligned} c_e[n] = &(c_1(A_2 * c[n] + B_2) - (A_2 * c_e[n] + B_2) \\ &(A_2 * c[n] * c[n] + B_2) - c_3 c_e[n]) \times \frac{h}{\varepsilon_c \tau_c} + c_e[n+1] \end{aligned} \tag{32}$$

$$\begin{aligned} s_m[n+1] = &[(1 + A_1 * (s_{sm}((Z) - h_{sm})) + B_1) \\ &\times (1 - s_m[n]) - \frac{s_m[n]}{ds_m}] \times \frac{h}{\tau_{sm}} + s_m[n] \end{aligned} \tag{33}$$

$$\begin{aligned} G_m[n+1] = &[(1 + A_1 * (s_{Gm}(c[n] - h_{Gm})) + B_1) \\ &\times (1 - G_m[n]) - \frac{G_m[n]}{dG_m}] \times \frac{h}{\tau_{Gm}} + G_m[n] \end{aligned} \tag{34}$$

The values of all parameters in Eqs. (31)–(34) are taken from [19] and reported in Table 3, while we also considered SCM technique. The discrete equations of the astrocyte mathematical model are as follows [18]:

$$x[n+1] = (-x[n] + 0.05 + 1.5y[n])h + x[n] \quad (35)$$

$$y[n+1] = ((1 + (a[Z[n] - 2] + b)(1 - y[n]) - 2y[n]) \times h + y[n] \quad (36)$$

The values of all parameters in Eqs. (35) and (36) are taken from [18]. Finally the discrete equations of the proposed model are as follows:

$$x[n+1] = (-x[n] + 0.05 + 1.5y[n])h + x[n] \quad (37)$$

$$y[n+1] = (0.0937Z[n] - 2.035y[n] + 0.03593)h + y[n] \quad (38)$$

Figure 7 shows the scheduling diagrams for each discrete equations of the astrocyte biophysical model in one iteration. This process is performed for producing each output sample using last samples. In our digital design, a memory register is used at each output block. It stores the outputs which will be used in the next calculations. Individual state variables are

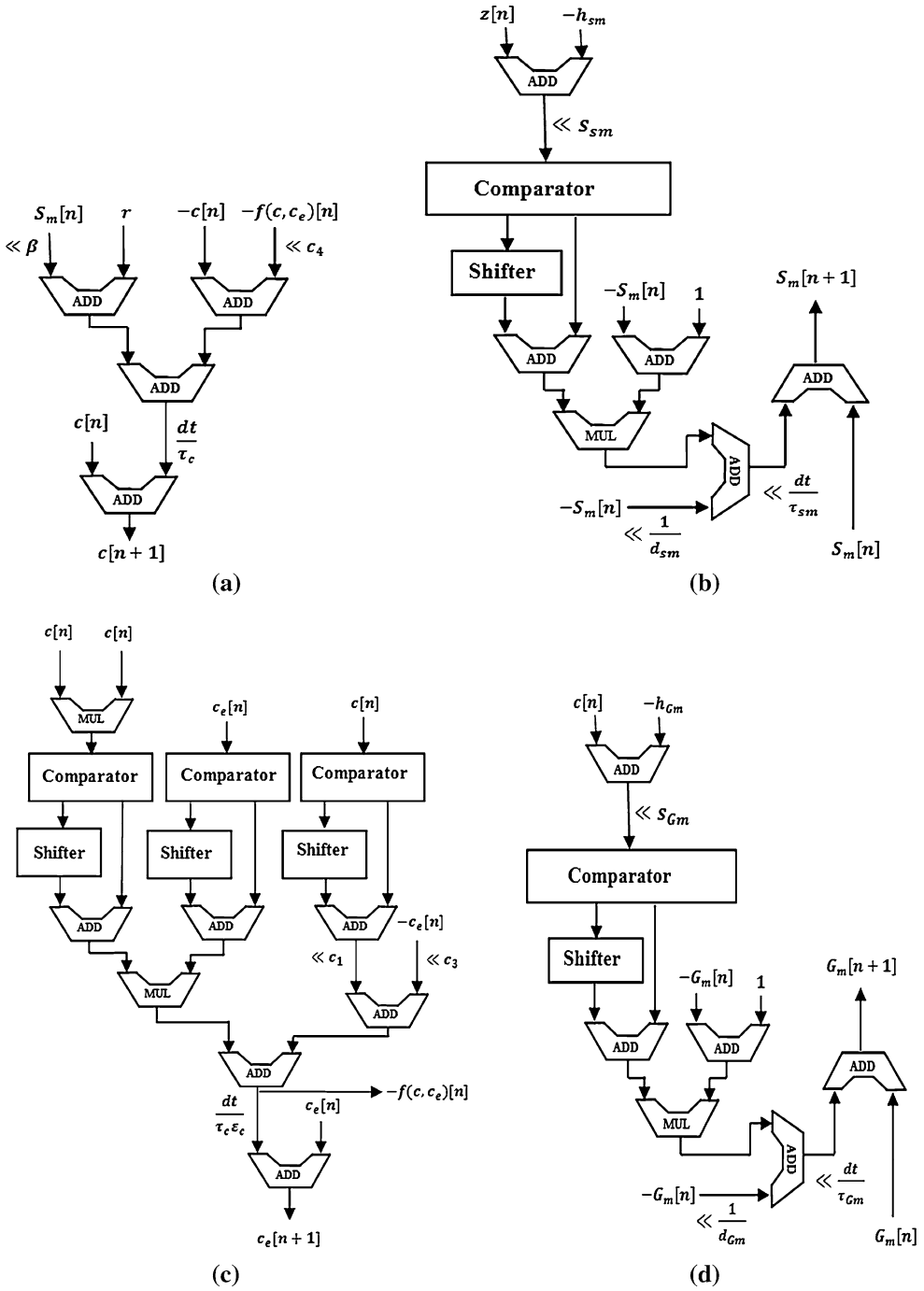

Fig. 7 Scheduling diagram of the astrocyte biophysical model. **a** Calcium concentration in the astrocyte cytoplasm, c, **b** the second messenger IP_3, S_m, **c** calcium concentration within the endoplasmic reticulum, c_e **d** astrocyte output, G_m

solved in n-bits registers which can be determined based on the required precision for implementation. In our research, $n = 20$ (4 bits for integer part and 16 bits for fractional part). The appropriate A_i and B_i [Eqs. (31)–(34)] are taken from [19] in order to approximate nonlinear function [19].

The scheduling diagrams for individual discrete equations of the astrocyte mathematical model [Eqs. (35), (36)] and the proposed stimulator [Eqs. (37), (38)] are shown in Figs. 8 and 9, respectively. As can be seen from Fig. 9, the proposed model enables us to design an area-efficient multiplier-less hardware architecture to be implemented on the FPGA.

The three digital circuits of stimulators are synthesized using Xilinx ISE tools, and the resource utilization of the FPGA implementations is summarized in Table 4.

Based on the stability analysis discussed in Sect. 3.3, the new proposed stimulator model has the dynamic behavior similar to the astrocyte mathematical model, while compared to the other stimulators, it is an efficient, low-cost digital hardware. So in the next section, we consider the new proposed model as a bio-inspired stimulator in the closed-loop DBS system to investigate its performance in preserving normal activity of the cortical network.

5 Results of simulations and hardware implementation

Since the proposed bio-inspired stimulator can be designed multiplier-less and then fabricated on digital platform with low implementation cost, we report the result of applying this new stimulator on neural population model.

Software and hardware simulations have been done by Visual Studio and ModelSim. We want to investigate the performance of the proposed stimulator by turning it ON and OFF. Stimulator must be able to break the hyper-synchronous firing of the large-scale network of neurons. External input is increased to create abnormally synchronized regime in the time interval 7000–14,000 ms and is shown in Fig. 10. The time-varying rate of spike trains is considered as the input from thalamus to the cortical population whose input signal is superposition of a time-varying rate of Poissonian spike trains and a noise component. Signal and noise are shown in blue and red, respectively.

First, we consider the case when stimulator is not utilized yet. In other words, $\lambda = 0$ in Fig. 3. Activities of the pyramidal neurons have shown in Fig. 11. Figure 11a shows the raster plot of the activity of pyramidal neurons (neurons have the highest firing rate during the time interval 7000–14,000 ms). Recorded LFP from pyramidal neurons is shown in Fig. 11b, and Fig. 11c shows the number of spikes (computed in a 400 ms bin), as a measure of synchronization of neurons. This figure shows that neural oscillations become more pronounced, and hyper-synchronous firing of neurons occur when the input signal rate increases.

Epilepsy is characterized by spontaneous seizures due to hyper-excitability and hyper-synchrony of cortical brain neurons [49]. We introduce proposed stimulator as a technique for effective de-synchronization. In order to show the ability of the bio-inspired stimulator to avoid the self-sustained oscillations in neural population, we consider the

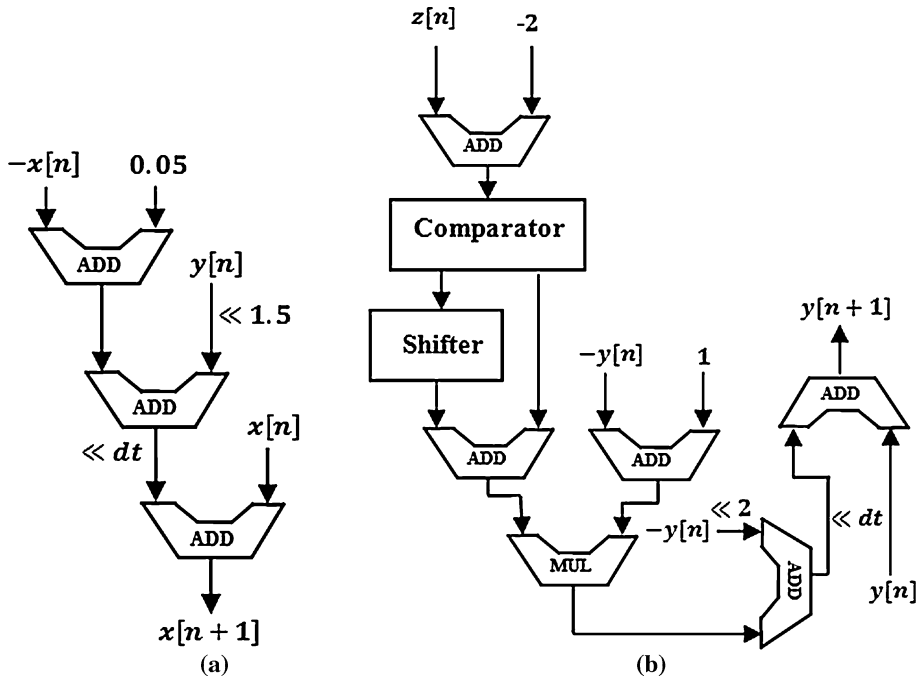

Fig. 8 Scheduling diagram of the astrocyte mathematical model, **a** the x-dynamic and **b** the y-dynamic

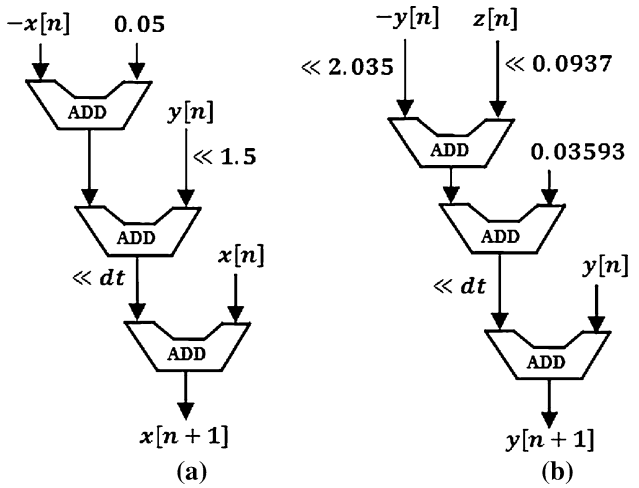

Fig. 9 Scheduling diagram of the proposed stimulator, **a** the *x*-dynamic and **b** the *y*-dynamic. As is evident, the proposed stimulator can be designed multiplier-less

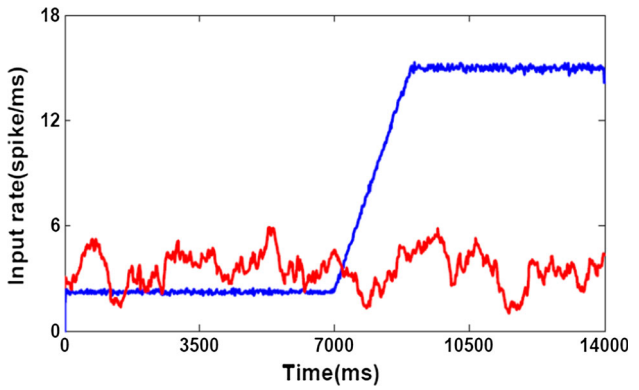

Fig. 10 A time-varying rate of Poissonian spike trains representing external inputs to each neuron in the network. The input is superposition of a "signal" and a "noise" component. The "signal" is shown in *blue* and the noise is shown in *red* (color figure online)

closed-loop system in Fig. 3 ($\lambda \neq 0$). To terminate pathological synchronization in the time interval 7000–14,000 ms, we apply the proposed stimulator from the beginning of simulation as shown in Fig. 12. Figure 12a, b shows the LFP signal and stimulator output current, respectively. Also, Fig. 12c, d shows the raster plot of the pyramidal neurons firing and number of spikes (computed in a 400 ms bin) of pyramidal neurons, respectively. As the results indicate, proposed stimulator can perform quite well, and in spite of abnormal increase in the cortical excitatory input, the normal ongoing activities continue. Hence, the bio-inspired stimulator can provide appropriate feedback control in suppressing excessive synchronous neural activity, while it has no undesirable effects on normal behavior of neurons (the time interval of 0–7000 ms).

In order to evaluate the performance of the proposed stimulator, we turn on the stimulator at different times. In Fig. 13, the proposed stimulator is OFF during time interval 0–10,000 ms and it will be turn on during time interval 10,000–14,000 ms. The LFP of the network, stimulator output current, the raster plot of the firing activity of pyramidals and number of spikes (computed on a 400 ms bin) of pyramidals are shown in Fig. 13a–d, respectively.

Finally, we investigate the performance of the bio-inspired stimulator when it will be switched ON at $t = 8000$ ms and $t = 11000$ ms and OFF at $t = 9000$ ms, $t = 12500$ ms, intermittently. Figure 14 shows the results in which the good performance is clear.

Considering Figs. 12, 13 and 14, the bio-inspired stimulator can eliminate the pathological neuronal synchronization when the cortical input is high, but as the stimulator is switched OFF, abnormally synchronized regime reappears again. As a result, it can be suggested that stimulator could be a candidate as a new DBS technique, but its performance in real neural network should be more analyzed. One of the most advantages of the bio-inspired stimulator is its on-demand characteristics which makes it possible for real clinical applications [50]. Moreover, the new proposed stimulator can omit excessive synchronization without any undesired impacts on the model intrinsic characteristics and normal ongoing activities of the cortical population. In fact, stimulator can shift the neuronal ensemble from abnormally synchronized regime to a desynchronized regime with an adaptive mechanism. When the abnormal firing activities change to the desynchronized oscillations, the input (z) gets close to zero and this leads to the decrease in the stimulator output current (x). It means that as the abnormal synchronization reduces, the amplitude of stimulation current significantly decreases.

In line with software simulations, to confirm the performance of the proposed digital stimulator, in Fig. 15 we turn OFF and ON the stimulator in ModelSim simulation of the corresponding digital circuit. Similar to our previous results, when the cortical input is high and the stimulator is switched OFF, the abnormal oscillations in population output appeared (Fig. 15a). But as the stimulator is switched ON again, the normal activity is emerged (Fig. 15b).

To evaluate the performance of the digital stimulator on hardware platform, it has been implemented on the Zed-Board development kit. The expandability features of this evaluation and development platform make it ideal for rapid prototyping and proof-of-concept development. The primary objective is to examine the feasibility of FPGA implementation of the model and to show that the hardware can reproduce the model responses. The system is developed under the Xilinx ISE 14 Foundation Design Software Environment using Verilog HDL. Figure 16 displays

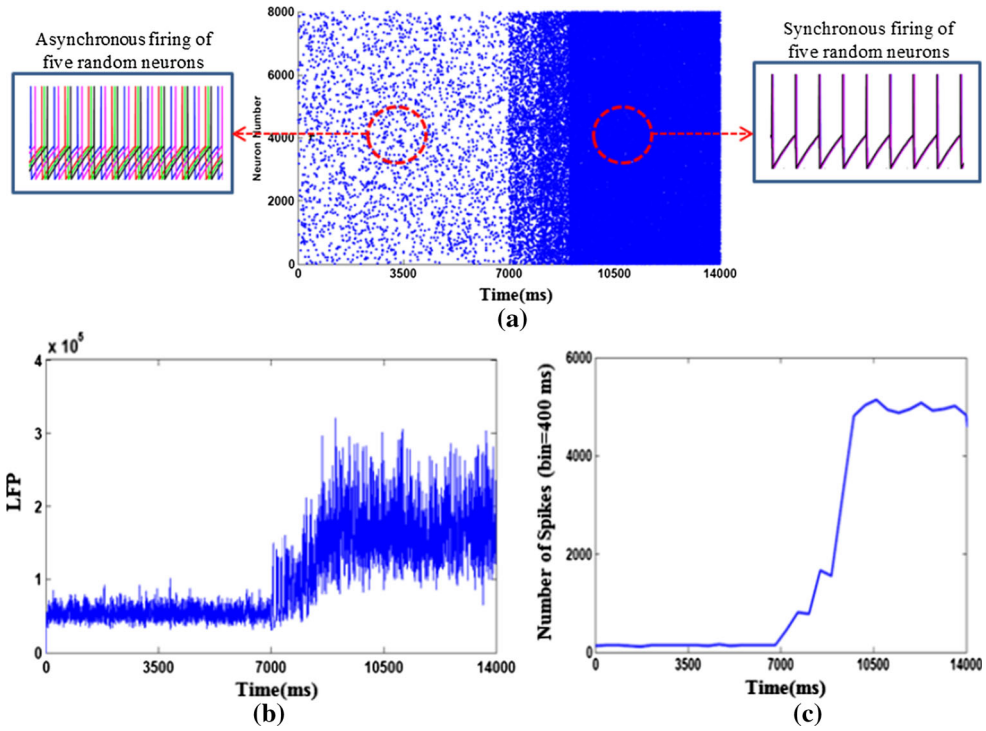

Fig. 11 Activity of the pyramidal neurons in form of **a** Raster plot of pyramidal neurons. **b** LFP of the network. **c** Number of spikes in a 400 ms bin. We can see pathophysiologic neural synchronization over a time interval (7000–14,000 ms) and normal activity in other time interval. Therefore, abnormal activity appeared in the network when the input rate increases for $\lambda = 0$

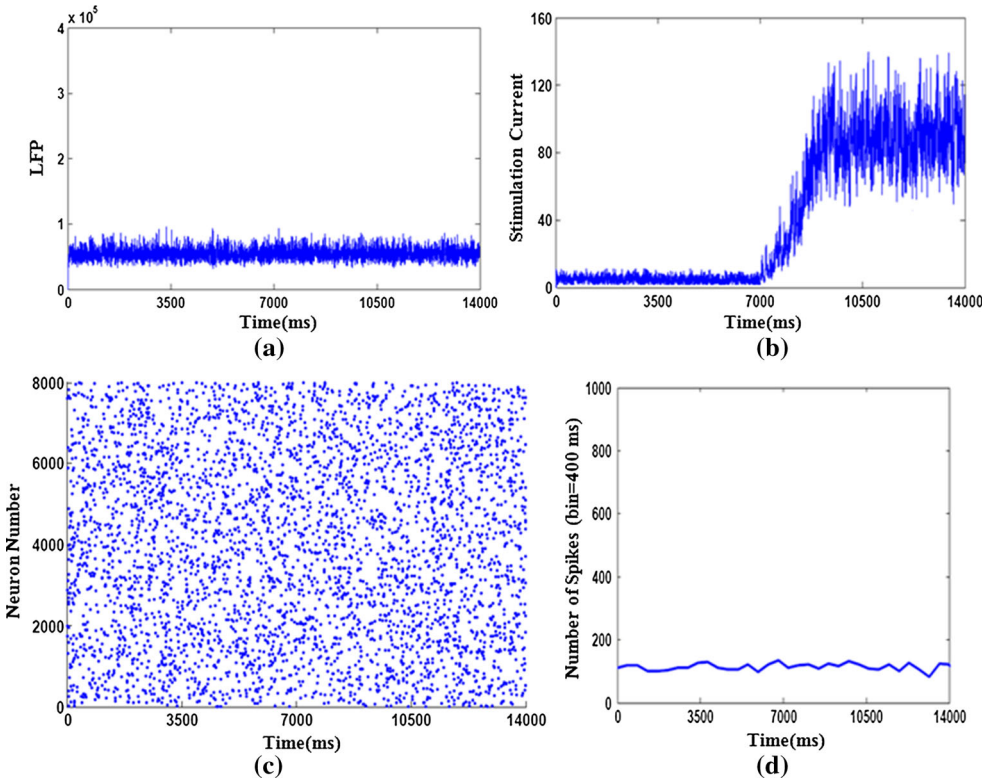

Fig. 12 Output activity from neural population and the proposed bio-inspired stimulator. **a**, **b** The LFP signal of the network and the stimulator output current, when the stimulator is ON from the beginning of simulation. **c**, **d** Output activity of the cortical population in the form of raster plot and number of spikes as a synchronization index. It is apparent the new proposed stimulator provides appropriate feedback action to the neuronal population model in closed-loop system which in turn prevents from the excessive activity, while it does not have any undesirable effects on the behavior of system

oscilloscope photographs of the digital implementation of the bio-inspired stimulator using VGA support on the ZedBoard. In this figure, we show that when the stimulator is switched OFF and the excitatory input signal is high, excessive synchronous firing of neurons appeared. Subsequently if the digital stimulator is switched ON again,

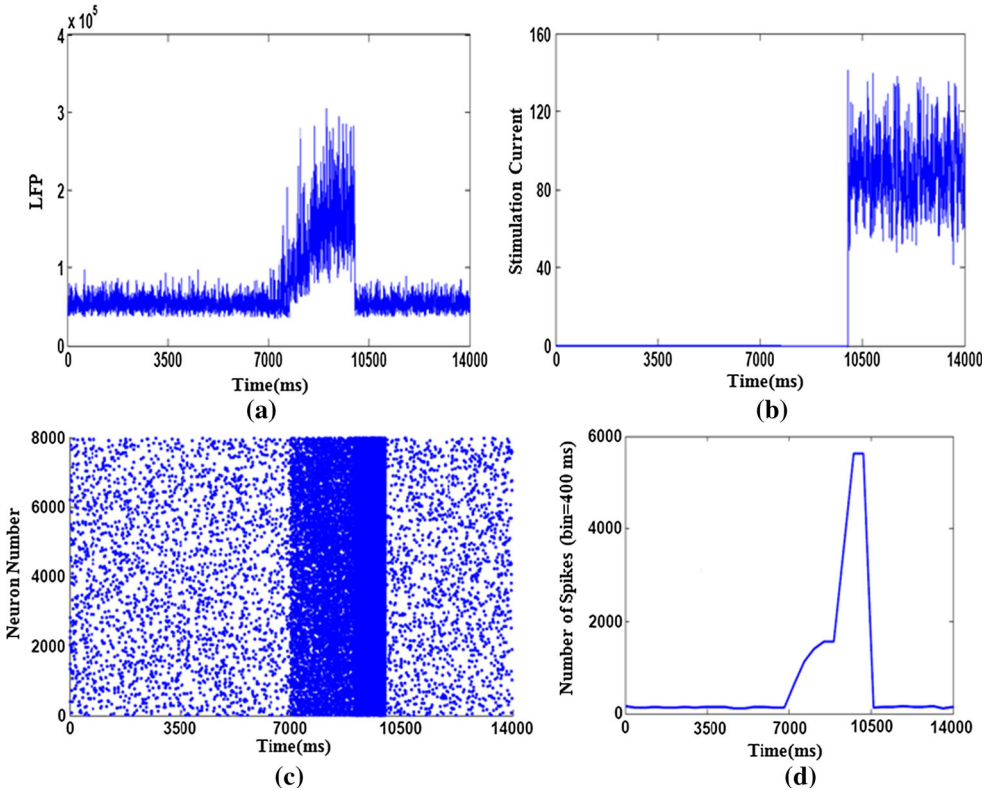

Fig. 13 Activity of the pyramidal neurons and stimulator output current when the stimulator is switched ON in 10,000 ms. **a** The LFP of the network, **b** stimulator output current, **c** raster plot of the firing activity of pyramidal neurons, **d** number of spikes (computed on a 400 ms bin). As can be seen, stimulator can avoid hyper-synchronous neuronal activities

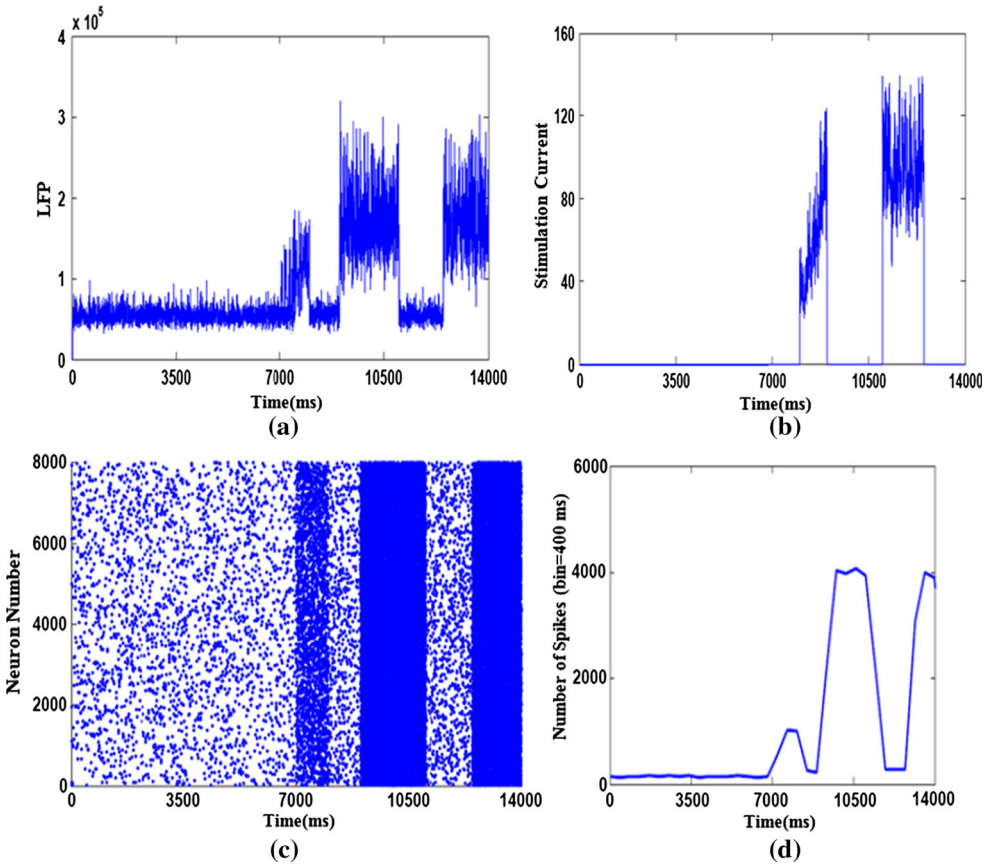

Fig. 14 The output activity of the network and stimulator when the proposed stimulator is switched ON and OFF intermittently. **a** The LFP of the network, **b** stimulator output current, **c** raster plot of the firing activity of pyramidal neurons and **d** number of spikes of pyramidal neurons. This figure shows that when the stimulator is activated, it prevents from hyper-synchronous activity

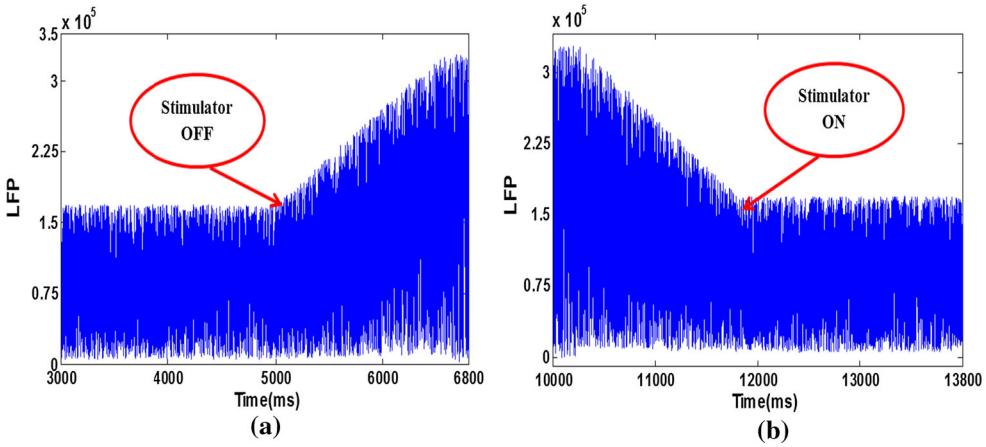

Fig. 15 The results of hardware simulation of the designed digital circuit for the closed-loop system in Fig. 3. **a** The shift from normal to abnormal activity for the cortical population output when the input is high and digital stimulator is switched OFF, and **b** the return to normal activity for the cortical output when the stimulator is switched ON

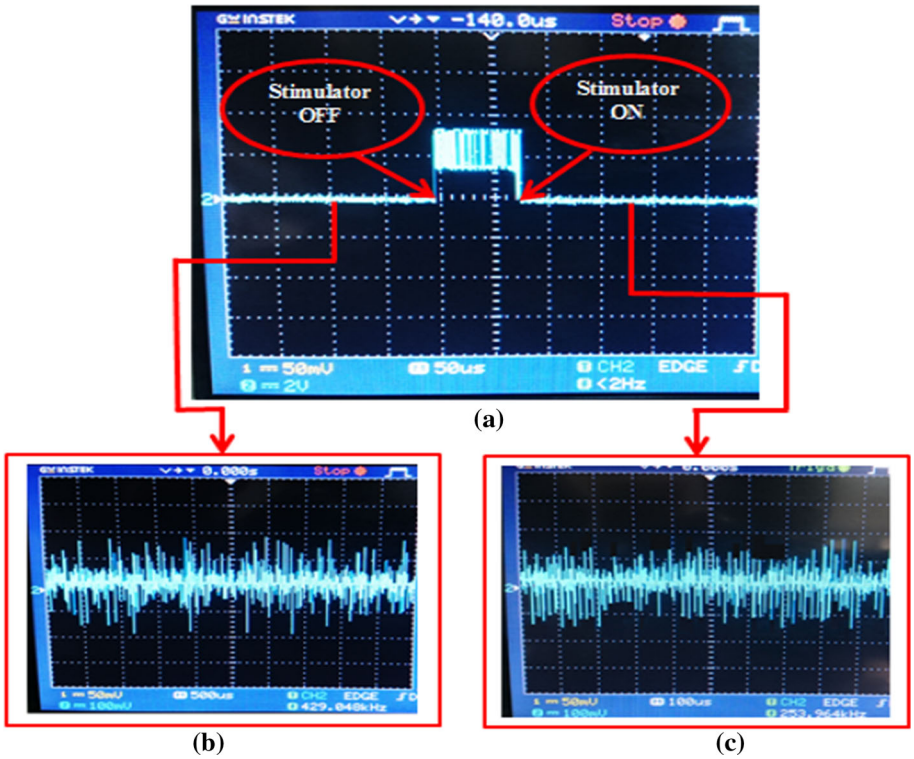

Fig. 16 The results of hardware implementation of the designed digital stimulator in the closed-loop system on the ZedBoard development board. **a** The appearance of high-amplitude neuronal oscillations, when the stimulator is OFF. Time and volt divisions of the oscilloscope are set on 50 μs and 2 V, respectively. **b**, **c** The normal activity of cortical population when the stimulator is ON. Here, volt divisions of the oscilloscope are set on 100 mV

despite of high input rate, stimulator circuit can apply the appropriate stimulation signal and prevents the occurrence of high-amplitude oscillations.

6 Conclusion

In the nervous system, synchronization processes play an important role, e.g. in the context of information processing and motor control. However, pathological, hyper-synchronization may impair brain function, so that epilepsy has been historically seen as a functional brain disorder associated with excessive synchronization of neuronal populations [42]. DBS usually is utilized to treat the diseases with intermittently hyper-synchronized neural oscillations such as epilepsy. In open-loop stimulation, implanted electrodes deliver electrical impulses continuously and independent of any feedback. Therefore, to achieve the best performance for DBS, we should design closed-loop stimulation technique (demand-controlled deep brain stimulation) with appropriate

control feedback [51]. In this paper, we proposed a bio-inspired stimulator and its digital circuit based on the mathematical model of the astrocyte. In order to evaluate the performance of the proposed stimulator, we provided a large platform based on the computational model of the cortical neurons that consist of 8000 pyramidal neurons, 2000 interneurons and 10 million excitatory and inhibitory synapses. Results of simulations and hardware FPGA implementation on the ZedBoard development kit verified that the proposed bio-inspired stimulator can effectively prevent the self-sustained high-amplitude oscillations, while compared to the other stimulators, it has more efficient digital circuit with a "demand-controlled" characteristic.

Acknowledgments This work was supported by the Iran National Science Foundation.

References

1. Singer W (1999) Neuronal synchrony: a versatile code for the definition of relations? Neuron 24(1):49–65
2. Jiruska P, de Curtis M, Jefferys JG, Schevon CA, Schiff SJ, Schindler K (2013) Synchronization and desynchronization in epilepsy: controversies and hypotheses. J Physiol 591(4):787–797
3. Blenkinsop A (2013). Computational modelling of normal function and pathology in neural systems: new tools, techniques and results in cortex and basal ganglia. Doctoral dissertation, University of Sheffield
4. Amiri M, Bahrami F, Janahmadi M (2011) Functional modeling of astrocytes in epilepsy: a feedback system perspective. Neural Comput Appl 20(8):1131–1139
5. WHO. Epilepsy (updated October 2012; cited 2009 December 8). http://www.who.int/mediacentre/factsheets/fs999/en/
6. Engel J Jr (2013) Why is there still doubt to cut it out? Epilepsy Curr 13:198–204
7. Engel J, McDermott MP, Wiebe S et al (2012) Early surgical therapy for drug-resistant temporal lobe epilepsy: a randomized trial. JAMA 307:922–930
8. Beleza P (2009) Refractory epilepsy: a clinically oriented review. Eur Neurol 62:65–71
9. Laxpati NG, Kasoff WS, Gross RE (2014) Deep brain stimulation for the treatment of epilepsy: circuits, targets, and trials. Neurotherapeutics 11(3):508–526
10. Sironi VA (2011) Origin and evolution of deep brain stimulation. Frontiers Integr Neurosci 5:42. doi:10.3389/fnint.2011.00042
11. Tukhlina N, Rosenblum M (2008) Feedback suppression of neural synchrony in two interacting populations by vanishing stimulation. J Biol Phys 34(3–4):301–314
12. Omel'chenko OE, Hauptmann C, Maistrenko YL, Tass PA (2008) Collective dynamics of globally coupled phase oscillators under multisite delayed feedback stimulation. Phys D Nonlinear Phenom 237(3):365–384
13. Rosin B, Slovik M, Mitelman R, Rivlin-Etzion M, Haber SN, Israel Z (2011) Closed-loop deep brain stimulation is superior in ameliorating parkinsonism. Neuron 72(2):370–384
14. Priori A, Foffani G, Rossi L, Marceglia S (2013) Adaptive deep brain stimulation (aDBS) controlled by local field potential oscillations. Exp Neurol 245:77–86
15. Amiri M, Montaseri G, Bahrami F (2011) On the role of astrocytes in synchronization of two coupled neurons: a mathematical perspective. Biol Cybern 105(2):153–166
16. Ranjbar M, Amiri M (2015) An analog astrocyte–neuron interaction circuit for neuromorphic applications. J Comput Electron 14(3):694–706
17. Ranjbar M, Amiri M (2015) Analog implementation of neuron–astrocyte interaction in tripartite synapse. J Comput Electron. doi:10.1007/s10825-015-0727-8
18. Nazari S, Faez K, Karami E, Amiri M (2014) A digital neuromorphic circuit for a simplified model of astrocyte dynamics. Neurosci Lett 582:21–26
19. Nazari S, Faez K, Amiri M, Karami E (2015) A novel digital implementation of neuron–astrocyte interactions. J Comput Electron 14(1):227–239
20. Nazari S, Faez K, Amiri M, Karami E (2015) A digital implementation of neuron–astrocyte interaction for neuromorphic applications. Neural Netw 66:79–90
21. Nazari S, Amiri M, Faez K, Amiri M (2015) Multiplier-less digital implementation of neuron–astrocyte signalling on FPGA. Neurocomputing 164:281–292
22. Nazari S, Amiri M, Faez K, Karami E (2014) A novel digital circuit for astrocyte-inspired stimulator to desynchronize two coupled oscillators. In: 2014 21th Iranian Conference on Biomedical Engineering (ICBME), IEEE, pp 80–85
23. Mazzoni A, Panzeri S, Logothetis NK, Brunel N (2008) Encoding of naturalistic stimuli by local field potential spectra in networks of excitatory and inhibitory neurons. PLoS Comput Biol 4(12):e1000239
24. Bertram EH (2013) Neuronal circuits in epilepsy: Do they matter? Exp Neurol 244:67–74
25. Stefanescu RA, Shivakeshavan RG, Talathi SS (2012) Computational models of epilepsy. Seizure 21(10):748–759
26. Paz JT, Davidson TJ, Frechette ES, Delord B, Parada I, Peng K et al (2013) Closed-loop optogenetic control of thalamus as a tool for interrupting seizures after cortical injury. Nat Neurosci 16(1):64–70
27. Frohlich F, Timofeev I, Sejnowski TJ, Bazhenov M (2008) Extracellular potassium dynamics and epileptogenesis. In: Soltesz I, Staley K (eds) Computational Neuroscience in Epilepsy, pp 407–427
28. Kudela P, Franaszczuk PJ, Bergey GK (2003) Changing excitation and inhibition in simulated neural networks: effects on induced bursting behavior. Biol Cybern 88(4):276–285
29. Winestone JS, Zaidel A, Bergman H, Israel Z (2012) The use of macroelectrodes in recording cellular spiking activity. J Neurosci Methods 206:34–39
30. Weinberger M, Hutchison WD, Dostrovsky JO (2009) Pathological subthalamic nucleus oscillations in PD: Can they be the cause of bradykinesia and akinesia? Exp Neurol 219:58–61
31. Sancristóbal B, Vicente R, Garcia-Ojalvo J (2014) Role of frequency mismatch in neuronal communication through coherence. J Comput Neurosci 37(2):193–208
32. Barardi A, Malagarriga D, Sancristobal B, Garcia-Ojalvo J, Pons AJ (2014) Probing scale interaction in brain dynamics through synchronization. Philos Trans R Soc B Biol Sci 369(1653): 20130533
33. Cavallari S, Panzeri S, Mazzoni A (2014) Comparison of the dynamics of neural interactions between current-based and conductance-based integrate-and-fire recurrent networks. Frontiers Neural Circuits 8:12
34. Linne ML, Jalonen TO (2014) Astrocyte-neuron interactions: from experimental research-based models to translational medicine. Prog Mol Biol Transl Sci 123:191
35. Clarke LE, Barres BA (2013) Emerging roles of astrocytes in neural circuit development. Nat Rev Neurosci 14(5):311–321
36. Schafer DP, Lehrman EK, Kautzman AG, Koyama R, Mardinly AR, Yamasaki R et al (2012) Microglia sculpt postnatal neural circuits in an activity and complement-dependent manner. Neuron 74(4):691–705

37. Verkhratsky A, Nedergaard M (2014) Astroglial cradle in the life of the synapse. Philos Trans R Soc B Biol Sci 369(1654):20130595
38. Henneberger C, Papouin T, Oliet SH, Rusakov DA (2010) Long-term potentiation depends on release of D-serine from astrocytes. Nature 463:232–236
39. Halassa MM, Florian C, Fellin T, Munoz JR, Lee SY, Abel T, Haydon PG, Frank MG (2009) Astrocytic modulation of sleep homeostasis and cognitive consequences of sleep loss. Neuron 61:213–219
40. Seifert G, Steinhäuser C (2013) Neuron–astrocyte signaling and epilepsy. Exp Neurol 244:4–10
41. Amiri M, Bahrami F, Janahmadi M (2012) Modified thalamo-cortical model: a step towards more understanding of the functional contribution of astrocytes to epilepsy. J Comput Neurosci 33(2):285–299
42. Amiri M, Bahrami F, Janahmadi M (2012) On the role of astrocytes in epilepsy: a functional modeling approach. Neurosci Res 72(2):172–180
43. Postnov DE, Koreshkov RN, Brazhe NA, Brazhe AR, Sosnovtseva OV (2009) Dynamical patterns of calcium signaling in a functional model of neuron-astrocyte networks. J Biol Phys 35(4):425–445. doi:10.1007/s10867-009-9156-x
44. Montaseri G, Yazdanpanah MJ (2014) Desynchronization of two coupled limit-cycle oscillators using an astrocyte-inspired controller. Int J Biomath 7(01):1450001, 1–23
45. Touboul J, Brette R (2008) Dynamics and bifurcations of the adaptive exponential integrate-and-fire model. Biol Cybern 99(4–5):319–334
46. Khalil HK, Grizzle JW (2002) Nonlinear systems, vol 3. Prentice hall, Upper Saddle River
47. Majumder T, Pande PP, Kalyanaraman A (2014) Hardware accelerators in computational biology: application, potential and challenges. Design & Test, IEEE 31(1):8–18
48. Piri M, Amiri M, Amiri M (2015) A bio-inspired stimulator to desynchronize epileptic cortical population models: a digital implementation framework. Neural Netw 67:74–83
49. Devinsky O, Vezzani A, Najjar S, De Lanerolle NC, Rogawski MA (2013) Glia and epilepsy: excitability and inflammation. Trends Neurosci 36(3):174–184
50. Montaseri G, Yazdanpanah MJ, Bahrami F (2015) Designing a deep brain stimulator to suppress pathological neuronal synchrony. Neural Netw 63:282–292
51. Beuter A, Lefaucheur JP, Modolo J (2014) Closed-loop cortical neuromodulation in Parkinson's disease: An alternative to deep brain stimulation? Clin Neurophysiol 125(5):874–885